Asymmetries and cross sections for the reaction $\vec{p}+p\rightarrow p+\pi^{+}+n$ at 800 MeV

A. D. Hancock, R. W. Hackenburg, E. V. Hungerford, B. W. Mayes, L. S. Pinsky, J. C. Allred,* and T. M. Williams†
University of Houston, Houston, Texas 77004

S. D. Baker, J. A. Buchanan, J. M. Clement, M. Copel,‡ I. M. Duck, G. S. Mutchler, G. P. Pepin,§ E. A. Umland, and G. C. Phillips
T. W. Bonner Nuclear Laboratories, Rice University, Houston, Texas 77005

M. W. McNaughton and C. Hwang
Los Alamos National Laboratory, Los Alamos, New Mexico 87545

M. Furić
Institut "Ruder Bosković," Zagreb, Yugoslavia
(Received 8 November 1982)

Kinematically complete data (analyzing powers and polarized cross sections) for the reaction $\vec{p}+p\rightarrow p+\pi^{+}+n$ at 800 MeV have been accumulated at twelve angle pairs with polarized beam and unpolarized target. Analyzing powers as large as 0.6 are observed in the regions of phase space where the Δ^{++} resonant state can be produced. The four-momentum transfer to the proton-pion Δ^{++} resonance varied between 0.09 $(\mathrm{GeV}/c)^2$ to 0.81 $(\mathrm{GeV}/c)^2$. Current theories are not capable of reproducing these results in detail.

[NUCLEAR REACTIONS $\vec{p}(p,n)\pi^{+}p$, measured $d^3\sigma/dp_1 d\Omega_1 d\Omega_2$ and analyzing power.]

I. INTRODUCTION

The discovery of dramatic structure in the spin dependent proton-proton observables just above pion threshold has aroused interest in the spin effects in pion production mechanisms. Recent energy dependent measurements[1] of the total cross section differences for transverse ($\Delta\sigma_T$) and longitudinal ($\Delta\sigma_L$) pure spin states below 3000 MeV incident energy have led to the suggestion of dibaryon resonances in the proton-proton and $NN\pi$ systems. Hoshizaki[2] and Bhandari *et al.*,[3] through phase shift analyses, suggest dibaryon resonances in the $^1D_2$ and $^3F_3$ partial waves with invariant masses of 2175 and 2200 MeV, respectively. If such resonances exist, they are predicted to have large inelasticities ($\sim$0.8) and could be expected to show strong effects in the $p+p\rightarrow p+\pi^{+}+n$ channel. In addition, understanding the spin dependence of the reaction $p+p\rightarrow p+\pi^{+}+n$ is essential for understanding the proton-proton interaction around 800 MeV incident energy. At these energies the total proton-proton cross section contains a significant inelastic component due to the onset of pion production. These considerations have led to a number of kinematically complete pion production experiments. The KEK Group[4] has measured all *pp* interaction cross sections at 11 momenta from 0.9 to 2.0 GeV/*c* including the reactions $p+p\rightarrow p+\pi^{+}+n$ and $p+p\rightarrow p+p+\pi^{0}$, using a 1 m liquid hydrogen bubble chamber and an unpolarized beam. The Argonne National Laboratory–Rice University Group[5] has measured the asymmetry for the reaction $p+p\rightarrow p+\pi^{+}+n$ at four momenta from 1.2 to 2.0 GeV/*c* using the Argonne effective mass spectrometer with a polarized beam and an unpolarized target. The Leningrad Group[6] has measured $p+n\rightarrow p+p+\pi^{-}$ at nine incident proton energies from 500 to 1000 MeV using a 35 cm bubble chamber filled with liquid deuterium. Their paper gives only total cross sections. Older references can be found in Ref. 7.

The present experiment examines the reaction $\vec{p}+p\rightarrow p+\pi^{+}+n$ in a kinematically complete counter experiment with a polarized proton beam on an unpolarized proton target. In these measurements, the proton and π^{+} were detected in coincidence. Of the ten possible nucleon-nucleon single

pion production reactions, three have proton-proton initial states:

$$p+p \rightarrow p+\pi^+ +n \quad (1)$$

$$\rightarrow d+\pi^+ \quad (2)$$

$$\rightarrow p+p\ \pi^0 . \quad (3)$$

In principle, (1), (2), and (3) are always present in proton-proton collisions above the pion threshold. Because of limitations due to the kinematics and momentum acceptance of the spectrometer arm (see Sec. II), reaction (2) is not seen in the data described here. Therefore reaction (3) represents the only possibility for misidentification of reaction (1).

At 800 MeV incident proton energy, reaction (1) can proceed via three reaction modes (in addition to nonresonant background):

$$\left.\begin{array}{l} p+p \rightarrow \Delta^{++}+n \quad (4) \\ p+p \rightarrow \Delta^{+}+p \quad (5) \\ p+p \rightarrow d^{*}+\pi^{+} \quad (6) \end{array}\right\} \rightarrow p+\pi^+ +n .$$

In modes (4) and (5) the pion is formed in a resonant state with a nucleon giving a Δ^+ when resonating with the neutron or a Δ^{++} when resonating with a proton. In both cases the relative energy in the pion-nucleon system is approximately 160 MeV. The d^* in mode (6) represents the proton-neutron system with small relative energy (i.e., nucleon-nucleon final state interaction). The kinematic conditions were chosen such that mode (4) was dominant at all angle pairs.

II. EXPERIMENTAL SETUP

The experiment was conducted at the Los Alamos Meson Physics Facility (LAMPF) on the External Proton Beam (EPB) channel. The polarized H^- beam was produced by the LAMPF Lamb shift ion source. The incident proton beam was approximately 70% polarized in the vertical direction and had an energy of 800 ± 3 MeV. The target was unpolarized liquid hydrogen at 20 K in a Kapton flask (5.08 cm in diameter and 6.86 cm along the beam line).

The experimental setup (see Fig. 1) consisted of (1) a magnetic spectrometer for proton detection [two scintillators, a momentum analyzing magnet, and four multiwire proportional counters (MWPC's)] and (2) a time-of-flight (TOF) arm for pion detection (two scintillators and two MWPC's). The spectrometer and TOF arm were operated in coincidence to accumulate kinematically complete data. To ensure the best possible time-of-flight measurement on the TOF arm, fast scintillator (Pilot U) and constant fraction discrimination were used. The spectrometer had a momentum resolution of $\Delta p/p \simeq 2.5\%$. The angular acceptance was $\Delta\theta=\pm3.5°$ horizontal and $\Delta\phi=\pm3.0°$ vertical. The angular acceptance of the TOF arm was $\Delta\theta=\pm2.8°$ and $\Delta\phi=\pm2.0°$. Time-of-flight resolution on the spectrometer was 2.5 nsec full width at half maximum (FWHM) and 1.0 nsec FWHM on the TOF arm. The incident proton beam intensity was monitored with two ion chambers and a Faraday cup. The relative intensity and the system live time were monitored by a two arm scintillator telescope which viewed proton-proton elastic events from the production target. The scintillator telescope was rotated out of the horizontal plane to avoid obscuring the spectrometer and TOF arm. The position and profile of the incident proton beam on the target was monitored continuously with two integrating MWPC's.

The data were processed using standard NIM and CAMAC electronics[8] and stored on magnetic tape by a Digital Equipment Corp. PDP 11/45 computer. The MWPC's were read out when a strobe (fast logic $S1\cdot S2\cdot S3\cdot S4$) was received with at least some predetermined MWPC's having nonzero readouts. Pulse heights and time of flight (relative to $S3$) were recorded for all the scintillators. Both the analog to digital converter (ADC) starts and time to digital converter (TDC) starts were gated by the strobe signal. The ion chambers and Faraday cup used Ortec 439 current digitizers.

The beam polarization was measured with the LAMPF EPB polarimeter.[9] It consists of eight plastic scintillator assemblies viewing a thin (~3 mm) CH_2 target. Four pairs of scintillators at $\theta_{lab}=17°$ and 67° measured proton-proton coincidences in right, left, up, and down scattering. The right, left pairs are used to monitor the vertical polarization component of the beam. The up, down pairs monitor any horizontal polarization components of the beam (typically less than 5%). The analyzing power of this instrument at 800 MeV is 0.481 ± 0.002.[9] For further details on the experimental setup and data analysis, consult Ref. 10.

III. DATA ANALYSIS

Only events with one track per MWPC coordinate were analyzed. Any event with a zero or multiple readout from any of the 12 coordinates was rejected. Zero and multiple readouts were counted so that the individual coordinate data efficiencies as well as the total system data efficiency (typically 40%) could be calculated.

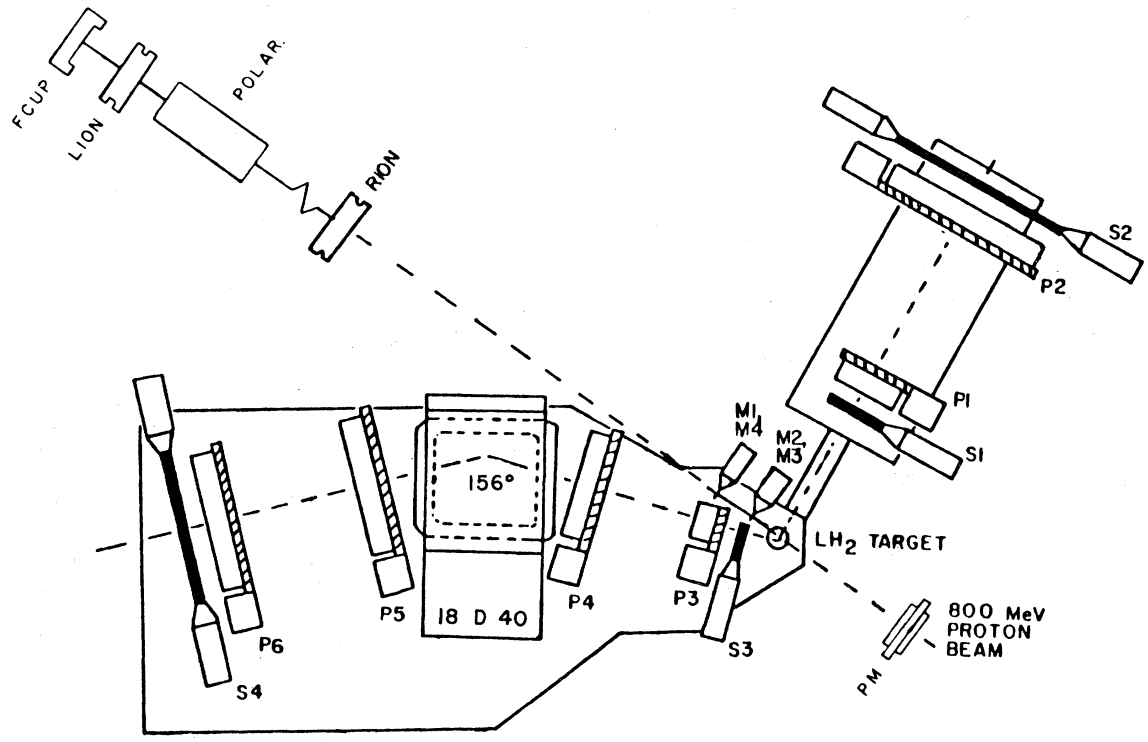

FIG. 1. The experimental setup. P_i=MWPC. S_i=scintillator. M_i=monitor scintillator. RION (LION)=Rice (LAMPF) ion chamber. PM=profile monitor. POLAR=polarimeter. 18-*D*-40=spectrometer magnet. FCUP=Faraday cup.

Several geometrical cuts were placed on the data. Using the TOF arm MWPC's and the first two MWPC's on the spectrometer arm, the vertex of the event at the target was calculated and subjected to appropriate cuts. Furthermore, the path of the proton through the spectrometer magnet was calculated using the two planes before and after the magnet. Events intersecting the pole tips were rejected. After the geometry of the event was checked, the momentum of the spectrometer arm particle was calculated using a uniform field approximation.

While the raw time-of-flight spectrum in the TOF arm gave some discrimination between protons and pions, the velocity spread possible in reactions (1) and (3) due to kinematic changes over the finite detector acceptance gave broad overlapping peaks. Background from reaction (3) was effectively eliminated by correcting the raw time-of-flight spectrum for this velocity spread. Assuming reaction (1), the observed angle and momentum in the spectrometer arm and the angle in the TOF arm completely determined the time of flight expected in the TOF arm. The measured TOF for events from reaction (1) are then close to this calculated value while events from reaction (3) are not grouped around this value. Figure 2 shows a typical spectrum of the difference between the measured TOF and the calculated TOF assuming reaction (1). The sharp peak at zero time difference provides good discrimination from the background.

Data were collected at 12 angle pairs over a wide range of the available phase space. Analyzing powers and cross sections were measured as a func-

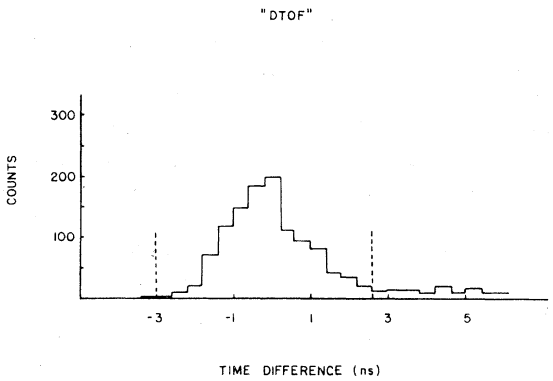

FIG. 2. The histogram for the difference in times of flight on the time of flight arm for a typical run. DTOF is the difference in the calculated and measured times of flight for the TOF arm. Cuts on DTOF are the primary method of eliminating background contamination.

tion of the final state proton momentum. Fifth order differential cross sections $(d^3\sigma/d\Omega_1 d\Omega_2 dp_1)$ were calculated for beam spin up and spin down. The cross section for the ith momentum bin is given by

$$\frac{d^3\sigma^{+(-)}}{d\Omega_1 d\Omega_2 dp_1} = N_{\rm cor}^{+(-)}(i)/N_I^{+(-)} N_T \Delta\Omega_i \Delta p \ , \quad (7)$$

where $N_{\rm cor}^{+(-)}(i)$=number of corrected events for spin up (down) in the ith momentum bin, N_T=number of target atoms per unit area (2.9×10^{23} atoms/cm^2), $N_I^{+(-)}$=number of incident polarized protons for beam spin up (down), $\Delta\Omega_1$=total system angle in the ith momentum bin, and Δp=final state proton momentum bin width (40 MeV/c). The total system solid angle per bin was calculated using a Monte Carlo program which took into account pion decay, geometry, and kinematics. The number of events were corrected for MWPC efficiencies, system dead time, and the beam polarization.

The analyzing power for the ith bin is defined as

$$A_y(i) = \frac{\sigma_i^+ - \sigma_i^-}{\sigma_i^+ + \sigma_i^-} \ , \quad (8)$$

where

$$\sigma^{+(-)} = d^3\sigma^{+(-)}/d\Omega_1 d\Omega_2 dp_1$$

for the ith bin.

In all cases the experiment was set up to detect a proton (in the spectrometer arm) scattered to the left looking downstream and a pion (in the TOF arm) scattered to the right. The sign of the analyzing power was then determined by spin up $(\vec{K}\times\vec{K}_p)$ minus spin down $(-\vec{K}\times\vec{K}_p)$ events (here $\vec{K}$ is the beam momentum direction and $\vec{K}_p$ is the final state proton momentum direction). The analyzing powers and their errors for the 12 angle pairs are given in Table I A–L as a function of the final state proton momentum. Table I also shows the fifth order differential cross section $(d^3\sigma/d\Omega_1 d\Omega_2 dp_1)$ for spin up and spin down and their errors. In most cases a large positive asymmetry is associated with the value of the final state proton momentum corresponding to the formation of a Δ^{++} resonance with subsequent decay. The spin averaged cross section for the angle pair 14.5°-21° agrees to within 15% of the unpolarized cross section of Hudomalj-Gabitzsch *et al.*[11] Also in Table I each angle is labeled with the Δ^{++} c.m. production angle θ_Δ, assuming a two body final state $p+p\to n+\Delta^{++}$. The momentum transfer to the Δ^{++} ranges from 0.09 GeV/c^2 at $\theta_\Delta=0°$ to 0.81 GeV/c^2 at $\theta_\Delta=90°$.

As a further consistency check for this experiment, the differential cross section $[d\sigma(\theta_{\rm c.m.})/d\Omega]$, and analyzing power $A_y(\theta_{\rm c.m.})$ for the elastic reaction $p+p\to p+p$ were measured periodically throughout the experiment. The results, given in Table II, agree with published differential cross sections and analyzing powers.[12]

IV. THEORETICAL MODELS

Umland and Duck[13] have attempted to fit the data using a peripheral model employing one pion exchange with a monopole form factor at the πNN vertex and with the full pion-nucleon–scattering amplitude included between the two πN vertices [see Fig. 3(a)]. Interfering with the one pion exchange graphs are one rho exchange graphs coupled to a Δ-resonance intermediate state [see Fig. 3(b)]. The ρNN and $\rho N\Delta$ vertices also include a monopole form factor.

The monopole form factor for the coupling constant $g_{\pi NN}$ is parametrized as a function of the four-momentum transfer t:

$$g_{\pi NN}(t) = f_{\pi NN}\left[\frac{2\pi_N}{m_\pi}\right]\frac{\Lambda_\pi^2 - m_\pi^2}{\Lambda_\pi^2 - t} \quad (9)$$

with $f_{\pi NN}=1.0$ (from Ref. 14), and a value of $\Lambda_\pi=1000$ MeV/c as determined by Dominquez and Clark[15] from charged pion photoproduction and by Dominquez and VerWest[15] from np and $\bar{p}p$ charge exchange scattering. The value of Λ_ρ was determined by fitting the present $p+p\to p+\pi^+ +n$ differential cross section data at $\theta_\Delta=0°$. A value of $\Lambda_\rho=1500$ MeV/c was found to give the best fit. The (virtual π) $N\to\pi N$ scattering amplitude was calculated using a partial wave analysis up to F waves.[16] The amplitude was taken off shell, following Rinat and Thomas,[17] with the continuation

$$e^{i\delta_{LJ}}\sin\delta_{LJ}\to e^{i\delta_{LJ}}\sin\delta_{LJ}\left[\frac{q_i}{q_f}\right]^2\left[\frac{q_f^2+\beta^2}{q_i^2+\beta^2}\right]^2 , \quad (10)$$

where $\beta=355$ MeV/c. The P_{33} wave was parametrized with the standard Breit-Wigner formula.

It should be noted that this model does not include the neutron-proton final state interaction. This interaction is most important for small neutron-proton relative energies. In this process kinematics restricts the final state proton momentum to the region below that of interest here. For example, at $\theta_{\rm proton}=21°$, $\theta_\pi=42.5°$, the final state proton momentum corresponding to minimum relative kinetic energy in the neutron-proton system is $p_{\rm proton}=580$ MeV/c. Umland and Duck restrict their theory to proton momenta above the neutron-

TABLE I. All cross section units are μb/sr^2 MeV/c.

Momentum	$d^3\sigma^+/d\Omega^2dp$	Error	$d^3\sigma^-/d\Omega^2dp$	Error	A_y	Error
	A. $\theta_{spec}=14.5°$, $\theta_{TOF}=42°$, Δ^{++} at 940 MeV, $\theta_\Delta=0°$					
460	1.79	0.25	1.75	0.24	0.011	0.099
500	2.57	0.31	3.76	0.32	−0.188	0.071
540	7.04	0.52	8.66	0.55	−0.103	0.048
580	10.48	0.51	12.40	0.51	−0.084	0.032
620	7.29	0.43	10.52	0.46	−0.181	0.036
660	4.58	0.35	7.16	0.37	−0.220	0.044
700	3.41	0.34	5.77	0.36	−0.257	0.055
740	3.67	0.35	4.76	0.35	−0.129	0.059
780	4.93	0.39	4.98	0.37	0.005	0.054
820	6.54	0.47	6.54	0.43	0.000	0.049
860	11.48	0.63	7.39	0.51	0.217	0.042
900	15.37	0.77	9.27	0.60	0.248	0.038
940	23.32	0.97	8.05	0.63	0.487	0.034
980	27.1	1.1	9.53	0.73	0.480	0.033
1020	22.8	1.1	6.73	0.66	0.544	0.038
1060	17.1	1.0	4.19	0.61	0.606	0.050
1100	7.54	0.73	0.94	0.41	0.778	0.088
	B. $\theta_{spec}=14.5°$, $\theta_{TOF}=21°$, Δ^{++} at 850 MeV, $\theta_\Delta=0°$					
380	2.83	0.51	3.81	0.54	−0.15	0.11
420	5.88	0.63	8.37	0.66	−0.175	0.064
460	9.91	0.85	16.9	1.00	−0.261	0.049
500	12.5	1.1	19.7	1.2	−0.224	0.051
540	12.1	1.1	15.5	1.2	−0.123	0.059
580	8.6	1.1	11.5	1.1	−0.144	0.078
620	9.6	0.78	13.92	0.85	−0.184	0.049
660	11.43	0.95	15.2	1.0	−0.142	0.052
700	15.3	1.0	18.4	1.0	−0.092	0.042
740	21.7	1.2	19.2	1.1	0.061	0.040
780	26.2	1.2	18.5	1.1	0.172	0.036
820	30.5	1.4	18.1	1.2	0.255	0.038
860	28.8	1.5	15.0	1.2	0.315	0.043
900	25.1	1.4	11.2	1.1	0.383	0.048
940	18.6	1.4	9.5	1.1	0.324	0.062
980	15.7	1.3	3.9	1.1	0.602	0.094
1020	9.2	1.2	3.0	1.1	0.51	0.14
1060	2.5	1.0	2.1	1.0	0.09	0.31
	C. $\theta_{spec}=19°$, $\theta_{TOF}=53°$, Δ^{++} at 1000 MeV, $\theta_\Delta=30°$					
380	2.08	0.53	2.48	0.48	−0.09	0.16
420	1.80	0.51	2.40	0.44	0.14	0.17
460	2.27	0.60	1.77	0.47	0.12	0.18
500	1.95	0.70	3.00	0.58	−0.21	0.19
540	4.21	0.87	3.87	0.76	0.04	0.14
580	3.46	0.53	3.89	0.44	−0.059	0.095
620	5.58	0.54	5.83	0.44	−0.022	0.061
660	4.32	0.47	5.44	0.41	−0.115	0.065
700	3.63	0.43	3.69	0.34	−0.008	0.075
740	2.47	0.38	1.65	0.30	0.20	0.11
780	2.59	0.40	1.47	0.28	0.28	0.11
820	3.61	0.43	2.06	0.31	0.273	0.088
860	4.62	0.52	1.89	0.36	0.419	0.91
900	6.91	0.61	2.85	0.41	0.416	0.070

TABLE I. (*Continued.*)

Momentum	$d^3\sigma^+/d\Omega^2dp$	Error	$d^3\sigma^-/d\Omega^2dp$	Error	A_y	Error
	C. $\theta_{spec}=19°$, $\theta_{TOF}=53°$, Δ^{++} at 1000 MeV, $\theta_\Delta=30°$					
940	11.01	0.77	3.31	0.44	0.538	0.053
980	14.92	0.92	4.55	0.56	0.533	0.049
1020	16.8	1.0	2.63	0.52	0.729	0.048
1060	6.61	0.71	2.30	0.43	0.484	0.083
	D. $\theta_{spec}=21°$, $\theta_{TOF}=42.5°$, Δ^{++} at 940 MeV, $\theta_\Delta=30°$					
500	1.15	0.24	1.20	0.17	−0.02	0.13
540	2.65	0.30	1.67	0.23	0.227	0.085
580	3.75	0.29	2.95	0.24	0.119	0.055
620	4.23	0.30	3.67	0.25	0.071	0.050
660	3.34	0.27	2.99	0.23	0.055	0.056
700	3.57	0.31	2.81	0.27	0.119	0.064
740	3.30	0.29	2.22	0.24	0.196	0.067
780	3.85	0.32	1.97	0.23	0.323	0.064
820	6.69	0.41	2.35	0.28	0.480	0.052
860	9.31	0.52	2.29	0.29	0.605	0.044
900	10.47	0.58	2.68	0.34	0.592	0.045
940	15.05	0.74	2.64	0.38	0.702	0.039
980	12.70	0.71	2.34	0.37	0.688	0.044
1020	7.63	0.58	1.09	0.31	0.750	0.064
1060	1.60	0.33	0.83	0.24	0.32	0.16
	E. $\theta_{spec}=18°$, $\theta_{TOF}=107°$, no Δ^{++}, $\theta_\Delta=60°$					
540	2.47	0.45	1.74	0.37	0.17	0.14
580	1.75	0.30	1.68	0.26	0.02	0.12
620	1.90	0.24	1.15	0.20	0.25	0.10
660	1.91	0.23	1.25	0.20	0.209	0.096
700	1.75	0.21	1.05	0.17	0.250	0.094
740	1.60	0.21	1.30	0.18	0.103	0.094
780	1.23	0.19	1.11	0.18	0.05	0.11
820	0.91	0.19	1.12	0.19	−0.10	0.13
860	0.27	0.17	1.20	0.20	−0.63	0.20
900	0.40	0.18	1.26	0.20	−0.52	0.17
940	0.55	0.20	1.33	0.24	−0.41	0.17
980	0.79	0.21	1.16	0.22	−0.19	0.16
1020	0.73	0.23	0.97	0.24	−0.14	0.19
	F. $\theta_{spec}=22.5°$, $\theta_{TOF}=75°$, Δ^{++} at 1010 MeV, $\theta_\Delta=60°$					
380	0.83	0.17	0.38	0.13	0.37	0.17
420	1.13	0.16	1.28	0.16	−0.062	0.094
460	1.57	0.20	1.75	0.20	−0.054	0.085
500	2.01	0.23	1.73	0.21	0.075	0.082
540	1.22	0.23	1.61	0.23	−0.14	0.12
580	1.47	0.19	1.62	0.18	−0.049	0.085
620	1.54	0.19	1.68	0.18	−0.043	0.082
660	1.52	0.17	1.18	0.15	0.126	0.083
700	1.75	0.18	1.08	0.16	0.237	0.085
740	1.27	0.18	0.91	0.15	0.17	0.11
780	0.65	0.16	0.54	0.12	0.09	0.16
820	0.65	0.16	0.87	0.15	−0.14	0.16
860	0.89	0.19	0.88	0.15	0.01	0.14

TABLE I. (*Continued.*)

Momentum	$d^3\sigma^+/d\Omega^2dp$	Error	$d^3\sigma^-/d\Omega^2dp$	Error	A_y	Error
	F. $\theta_{spec}=22.5°$, $\theta_{TOF}=75°$, Δ^{++} at 1010 MeV, $\theta_\Delta=60°$					
900	1.37	0.22	0.88	0.17	0.22	0.12
940	2.38	0.28	1.35	0.22	0.276	0.093
980	2.45	0.31	1.30	0.23	0.307	0.099
1020	0.44	0.19	0.38	0.15	0.07	0.29
	G. $\theta_{spec}=27.5°$, $\theta_{TOF}=45°$, Δ^{++} at 900 MeV, $\theta_\Delta=60°$.					
420	0.90	0.21	0.87	0.16	0.02	0.15
460	1.33	0.22	1.49	0.21	−0.06	0.11
500	1.54	0.26	1.78	0.26	−0.07	0.11
540	1.75	0.30	1.73	0.28	0.01	0.12
580	2.09	0.22	1.61	0.19	0.130	0.078
620	2.20	0.20	1.59	0.19	0.161	0.073
660	2.31	0.20	1.27	0.17	0.291	0.073
700	2.37	0.19	0.98	0.15	0.415	0.072
740	2.63	0.20	0.81	0.15	0.529	0.072
780	3.34	0.24	0.80	0.15	0.614	0.063
820	4.51	0.29	1.39	0.20	0.529	0.058
860	6.49	0.35	1.31	0.22	0.664	0.049
900	7.50	0.42	1.52	0.25	0.663	0.049
940	4.13	0.32	0.99	0.21	0.613	0.070
	H. $\theta_{spec}=29°$, $\theta_{TOF}=37°$, Δ^{++} at 850 MeV, $\theta_\Delta=60°$					
420	0.70	0.23	0.74	0.19	−0.03	0.21
460	0.80	0.23	0.96	0.24	−0.09	0.19
500	1.03	0.24	1.67	0.27	−0.24	0.13
540	0.96	0.27	1.26	0.28	−0.14	0.18
580	1.67	0.23	1.61	0.21	0.018	0.095
620	1.63	0.21	1.67	0.20	−0.012	0.088
660	2.02	0.21	1.55	0.19	0.132	0.079
700	2.48	0.24	1.39	0.20	0.282	0.080
740	2.60	0.23	1.24	0.19	0.354	0.077
780	3.76	0.26	1.51	0.19	0.427	0.059
820	5.27	0.30	1.38	0.20	0.584	0.051
860	5.26	0.32	1.61	0.21	0.531	0.052
900	3.62	0.28	1.15	0.18	0.518	0.064
940	2.01	0.27	0.73	0.20	0.47	0.11
	I. $\theta_{spec}=31°$, $\theta_{TOF}=21°$, Δ^{++} at 720 MeV, $\theta_\Delta=60°$					
500	2.13	0.61	4.88	0.75	−0.39	0.14
540	1.73	0.42	3.78	0.54	−0.37	0.12
580	1.63	0.37	3.60	0.45	−0.38	0.11
620	2.66	0.37	4.38	0.43	−0.244	0.080
660	3.87	0.39	4.65	0.40	−0.092	0.066
700	5.20	0.44	5.09	0.44	0.011	0.060
740	7.14	0.52	4.90	0.46	0.186	0.057
780	5.88	0.49	3.55	0.41	0.247	0.067
820	3.55	0.44	1.50	0.33	0.41	0.15
860	1.01	0.28	0.32	0.34	0.52	0.40
	J. $\theta_{spec}=29°$, $\theta_{TOF}=72°$, Δ^{++} at 500 MeV, $\theta_\Delta=90°$					
500	2.56	0.30	1.96	0.25	0.132	0.085
540	2.90	0.24	1.16	0.16	0.429	0.066

TABLE I. (*Continued.*)

Momentum	$d^3\sigma^+/d\Omega^2dp$	Error	$d^3\sigma^-/d\Omega^2dp$	Error	A_y	Error
	J. $\theta_{spec}=29°$, $\theta_{TOF}=72°$, Δ^{++} at 500 MeV, $\theta_\Delta=90°$					
580	2.26	0.19	1.24	0.13	0.291	0.061
620	1.96	0.16	0.88	0.11	0.380	0.064
660	1.71	0.15	0.684	0.098	0.429	0.069
700	1.34	0.14	0.639	0.098	0.354	0.081
740	1.32	0.14	0.65	0.10	0.340	0.082
780	1.08	0.14	0.85	0.11	0.119	0.090
820	1.43	0.17	0.98	0.13	0.187	0.086
860	1.14	0.17	0.70	0.12	0.24	0.11
	K. $\theta_{spec}=33°$, $\theta_{TOF}=50°$, Δ^{++} at 800 MeV, $\theta_\Delta=90°$					
460	2.27	0.57	2.72	0.61	−0.09	0.17
500	1.93	0.43	3.01	0.45	−0.22	0.13
540	3.04	0.43	2.10	0.36	0.18	0.11
580	2.75	0.35	1.93	0.31	0.175	0.099
620	2.87	0.35	1.28	0.28	0.38	0.11
660	2.49	0.34	0.71	0.24	0.56	0.13
700	3.71	0.40	0.89	0.31	0.61	0.11
740	4.63	0.45	0.82	0.28	0.699	0.091
780	4.03	0.48	1.19	0.30	0.544	0.098
820	2.99	0.43	0.89	0.30	0.54	0.13
	L. $\theta_{spec}=36.5°$, $\theta_{TOF}=35°$, Δ^{++} at 730 MeV, $\theta_\Delta=90°$					
500	1.46	0.32	2.45	0.37	−0.25	0.12
540	1.55	0.25	1.71	0.24	−0.05	0.11
580	2.00	0.23	2.17	0.22	−0.041	0.076
620	2.98	0.23	1.79	0.20	0.249	0.064
660	2.99	0.23	2.27	0.20	0.137	0.057
700	4.33	0.26	2.37	0.21	0.293	0.049
740	3.82	0.25	1.69	0.19	0.387	0.055
780	2.39	0.23	1.24	0.18	0.317	0.078

proton final state interaction region.

In addition to the basic peripheral model, Umland and Duck have also included effects due to the proposed $^1D_2$ and $^3F_3$ dibaryon resonance [Fig. 3(c)]. Hosizaki's[2] and Arndt's[3] phase shift analyses of nucleon-nucleon scattering suggest two inelastic resonances in the $^1D_2$, $I=1$, $J=2^+$, and $^3F_3$, $I=1$, $J=3^-$, partial waves. The masses of these resonances are estimated to be 2175 and 2200 MeV, respectively. To simplify the calculations, only the lowest partial waves were used for the $N\Delta$ final state system, namely, the $^5S_2$ state for the $^1D_2$ resonance and the $^5P_3$ state for the $^3F_3$ resonance. A Breit-Wigner form was assumed for the dibaryon amplitude. Further details of the calculation are given in Ref. 13. The relative phases of the amplitudes are not determined in the model; thus there is one adjustable parameter for each resonance.

The comparison of theory and experiments for selected angle pairs is given in Fig. 4. The peripheral model calculations are shown as a dashed line and peripheral model including dibaryons as a dot-dashed line. The peripheral model badly underestimates the cross section at large momentum transfer. In general, the calculated asymmetry shows little structure as a function of proton momentum, unlike the data which show considerable structure. The disagreement is worse at several angle pairs whose

TABLE II. Proton-proton calibration results.

Calibration run no.	$\theta_{spectrometer}=50°$, $\theta_{TOF}=30°$, $\theta_{c.m.}=70°$ $d\sigma/d\Omega$ (mb)	A_y
1	1.49±0.009	0.393±0.021
2	1.52±0.010	0.381±0.018
3	1.55±0.014	0.370±0.039
4	1.58±0.016	0.367±0.020
5	1.49±0.015	0.346±0.032
Ref. 11	1.55±0.05	0.371±0.003

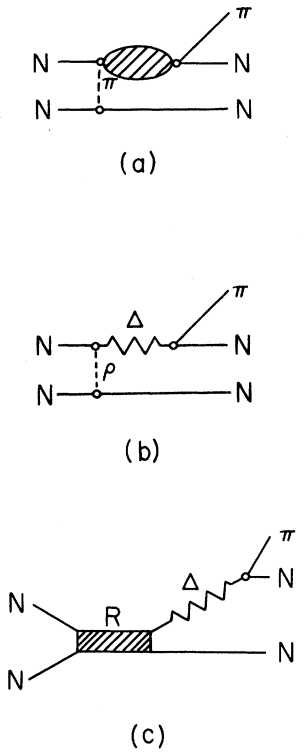

FIG. 3. The Feynman graphs for various single pion production processes. (a) shows the one pion exchange (OPE) contribution to single pion production. The intermediate state represented by the oval includes the full π-N scattering amplitude derived from π-N phase shift analyses (Refs. 13 and 16); (b) shows one-rho (two pion) exchange (ORE); (c) shows single pion production via a dibaryon resonance.

data are not shown (θ_p, θ_π=31°, 21°, and 21°, 42.5°, for example). While the inclusion of the dibaryon resonances improves the fits (dramatically in the case of θ_p,θ_π=14.5°, 42°), the overall effect is to increase the cross section and the magnitude of the asymmetry, but not to reproduce better the detailed structure of the data. Furthermore, the fits require different phase angles for each angle pair.

Dubach *et al.*[18] have calculated the analyzing power using a parameter-free, unitary model due to Kloet and Silbar.[19] This model is fully relativistic, includes all spin complications, and preserves both two and three body unitarity. However, it allows pion-nucleon interactions only through pion exchange in the $P_{11}(N^*)$ and $P_{33}(\Delta)$ partial waves. This model predicts substantially more structure in the analyzing powers than the peripheral model. It correctly predicts the analyzing powers for some angle pairs (θ_p,θ_π=31°, 21° and 36.5°, 35°, and, for $p_p > 700$ MeV/c, 18°, 107°, and 29°, 37°), but generally predicts values as much as 0.5 below the data at the other angle pairs.[20] The analyzing powers calculated from this model are shown in Fig. 4 as solid lines. Plots for additional angle pairs are given in Ref. 19.

A coupled channels model calculation by Betz *et al.*[21] uses effective potentials with form factors, including π, ρ, ω, σ, δ, η, and ϕ meson exchanges for the NN-NN interaction and π and ρ exchanges for the NN-$N\Delta$ interaction. Their model includes coupling the πd and NN channels and unitarity. With a suitable choice of cutoff parameters, Λ_π and Λ_ρ, they can reproduce the small momentum transfer data. They point out that the NN initial state interactions lower the cross sections by a significant amount, with the result that they obtain larger values for the cutoff parameter Λ_π (1200 MeV) than were found by Umland and Duck (1000 MeV). This is similar to the results of low energy nuclear physics where distorted-wave impulse approximation (DWIA) calculations give smaller cross sections in better agreement with the data than PWIA calculations. Betz *et al.* present calculations for the analyzing powers for two angle pairs ($\theta_p - \theta_\pi$=21°-42.5° and 31°-21°). In both cases their predictions are better than the peripheral model of Umland and Duck, but somewhat inferior to the results of Dubach *et al.* It should be noted that the authors state that the calculations are in progress and the results are preliminary.

V. CONCLUSIONS

The polarized differential cross sections $d^3\sigma/d\Omega_1 d\Omega_2 dp_1$ and analyzing powers for the reaction $\vec{p}+p\rightarrow p+\pi^+ +n$ have been measured as a function of final state proton momentum in a kinematically complete experiment at 800 MeV. The data exhibit strong angle and momentum dependent asymmetries, especially at proton momenta corresponding to the Δ^{++} resonance. Attempts to fit the analyzing power with a one-pion exchange peripheral model including form factors and one-rho exchange, and the full πN scattering amplitude have failed. The inclusion of the proposed $^1D_2$ and $^3F_3$ dibaryon resonances has met with very limited success at the cost of increasing the number of free parameters. The calculation of Dubach *et al.* indicates that two and three body unitary are needed to improve the calculation of the analyzing power, while the coupled channel calculations of Betz show that heavier meson exchanges and NN initial state interactions improve the fit to the spin

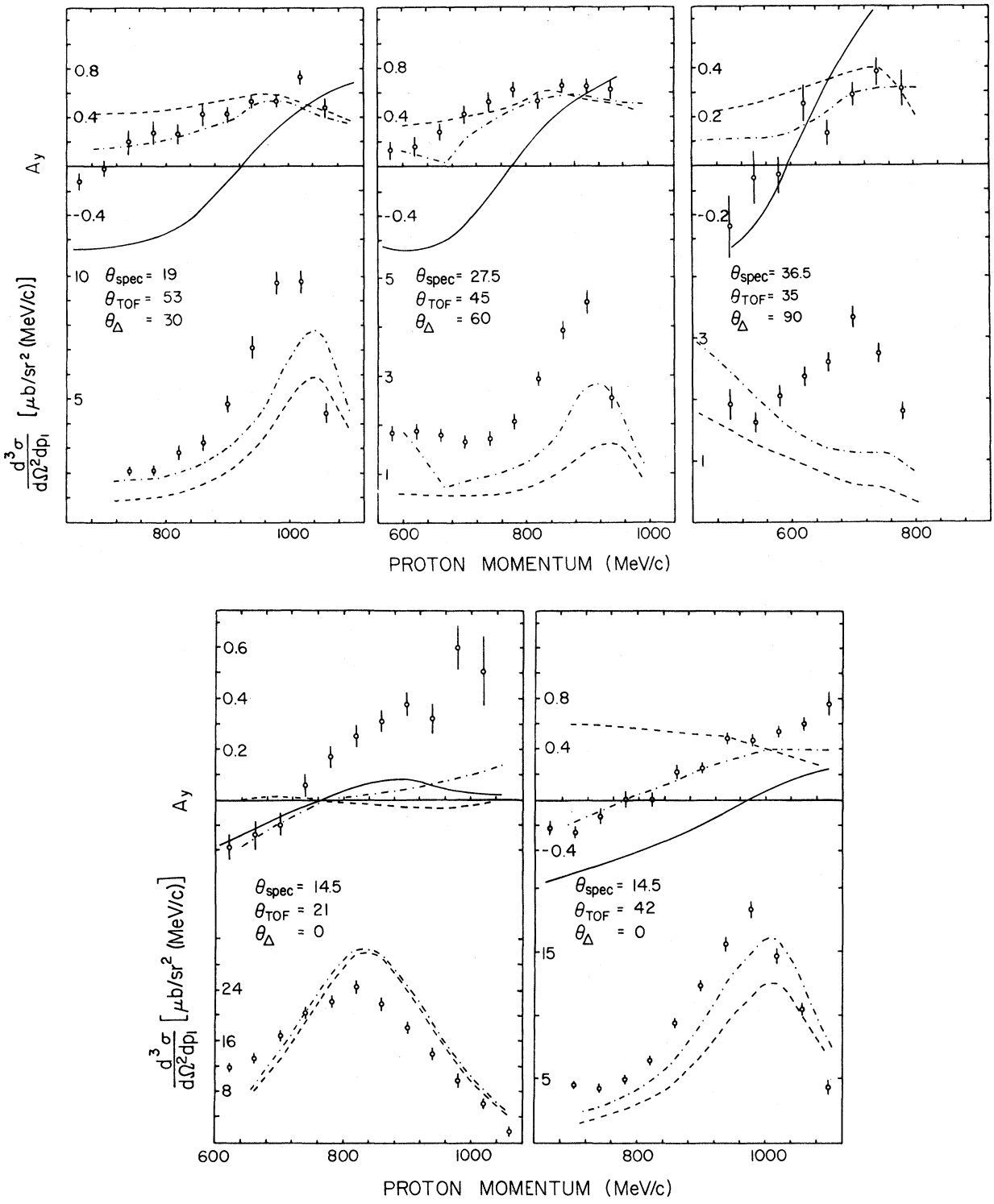

FIG. 4. The $p+p \rightarrow p+\pi^+ +n$ differential cross sections and analyzing power data are shown for selected angle pairs versus proton momentum. The peripheral model calculations of Umland *et al.* (Ref. 13) are shown as dashed lines and peripheral models including dibaryons as dot-dashed lines. Also shown as solid lines are the calculations of Dubach *et al.* (Ref. 18) for the analyzing powers.

averaged cross sections.

Both Dubach *et al.* and Betz *et al.* conclude that coupling to the $N\pi$ system produces rapid variation in the $^1D_2$ and $^3F_3$ scattering amplitudes and that it is unlikely that dibaryon states are needed. A simple explanation for the behavior of these partial waves has recently been published by VerWest.[22] Using a separable potential model coupled channel calculation, he is able to show that the looping character of the $^1D_2$ and $^3F_3$ amplitudes in the Argand diagram is due to the πN threshold behavior and not to nearby poles of the T matrix. Any dibaryon resonance in these partial waves would lie submerged under this structure. In order to determine if the present experiment is sensitive to dibaryons, much more accurate theoretical models will be needed.

ACKNOWLEDGMENTS

The authors wish to express their thanks to Louis Rosen and all the staff of the Los Alamos Meson Physics Facility for their help and cooperation. This work was supported by U.S. Department of Energy Contracts Nos. DE-AS05-77ER9-3948 and DE-AS05-81ER40032.

---

*Present address: Los Alamos National Laboratory, Los Alamos, NM 87545.

†Present address: Texaco Research Center, Bellaire, TX 77401.

‡Present address: Shell Development Co., Houston, TX 77005.

§Present address: Getty Oil Corp., Houston, TX 77070.

[1]See for example, A. Yokosawa, Phys. Rep. 65, 53 (1980). More recent results include J. Edginton, in *Polarization Phenomena in Nuclear Physics—1980 (Fifth International Symposium, Santa Fe)*, Proceedings of the Fifth International Symposium on Polarization Phenomena in Nuclear Physics, AIP Conf. Proc. No. 69, edited by G. G. Ohlsen, R. E. Brown, Nelson Jarmie, W. W. McNaughton, and G. M. Hale (AIP, New York, 1981); J. B. Roberts, *ibid.*, p. 31; H. Spinka, in Proceedings of the Workshop on Nuclear and Particle Physics at Energies Up to 31 GeV, Los Alamos National Laboratory Report LA8775-C, 1981 (unpublished); T. Kamae, Nucl. Phys. A374, 25C (1982).

[2]N. Hoshizaki, Prog. Theor. Phys. 61, 129 (1979).

[3]R. Bhandari *et al.*, Phys. Rev. Lett. 46, 1111 (1981).

[4]F. Shimizu *et al.*, Nucl. Phys. A386, 571 (1982).

[5]M. M. Calkin *et al.*, Bull. Am. Phys. Soc. 27, 552 (1982).

[6]L. G. Dakhno *et al.*, Phys. Lett. B114, 109 (1982).

[7]J. Bystricky and F. Lehar, Fachinformationzentrum, Karlsruhe, Data No. 11-1, 1978 (unpublished).

[8]J. Buchanan *et al.*, IEEE Trans. Nucl. Sci. 20, 691 (1972); J. Buchanan *et al.*, Nucl. Instrum. Methods 99, 159 (1972).

[9]M. McNaughton, Los Alamos National Laboratory Report No. LA-8307-Ms, 1980 (unpublished).

[10]A. D. Hancock, Ph.D. thesis, University of Houston, 1981 (unpublished).

[11]J. Hudomlaj-Gabitzsch *et al.*, Phys. Rev. C 18, 2666 (1978).

[12]H. Willard *et al.*, Phys. Rev. C 4, 1545 (1976); P. Bevington *et al.*, Phys. Rev. Lett. 41, 384 (1978).

[13]E. A. Umland, I. M. Duck, and G. S. Mutchler, see Ref. 1; E. A. Umland, M. A. thesis, Rice University, 1980 (unpublished).

[14]G. Brown and W. Weise, Phys. Rep. 22C, 279 (1975).

[15]C. Dominquez and B. VerWest, Phys. Lett. 89B, 333 (1980); C. Dominquez and R. B. Clark, Phys. Rev. C 21, 1944 (1980).

[16]R. Zidell, R. Arndt, and N. Roper, Phys. Rev. D 21, 1255 (1980).

[17]A. S. Rinat and A. W. Thomas, Nucl. Phys. A282, 365 (1977).

[18]J. Dubach *et al.*, Phys. Lett. 106B, 29 (1981).

[19]W. Kloet and R. Silbar, Nucl. Phys. A338, 231 (1980); A338, 317 (1980).

[20]R. Silbar, private communication.

[21]M. Betz *et al.*, TRIUMF Report No. TR1-81-59, 1981 (unpublished).

[22]B. VerWest, Phys. Rev. C 25, 482 (1982).